Integrated Kerr micro-comb sources for photonic microwave applications

Xingyuan Xu, David J Moss

Integrated Kerr micro-comb sources for photonic microwave applications

Xingyuan Xu and David J. Moss

[1]*Centre for Micro-Photonics, Swinburne University of Technology, Hawthorn, VIC 3122 Australia*

Abstract

We investigate the application of integrated micro-combs in RF photonic systems and demonstrate a microwave photonic intensity differentiator based on a Kerr optical comb generated by a compact integrated micro-ring resonator. The on-chip Kerr optical comb is CMOS-compatible and contains a large number of comb lines, which can serve as a high-performance multi-wavelength source for the transversal filter, thus greatly reduce the cost, size, and complexity of the system. The operation principle is theoretically analyzed, and experimental demonstrations of fractional-, first-, second-, and third-order differentiation functions based on the principle are presented.

Keywords: Optical frequency combs, micro-ring resonator, optical signal processing.

1. INTRODUCTION

Radio frequency (RF) and microwave photonics, which bring together the worlds of radiofrequency engineering and optoelectronics, exploit the potential of optical technologies and benefit RF systems in many respects, including high speed, broad operation bandwidth, low loss, and strong immunity to electromagnetic interference [1-6]. A diverse range of photonic approaches to RF signal generation, transmission, processing, and sensing have been proposed and widely employed in RF systems and communication networks [7-15]. Nevertheless, most RF systems are composed of discrete components, which impose certain drawbacks in terms of cost, power consumption and reliability, thus holding RF photonic systems from reaching maturity and replacing traditional RF solutions [16, 17]. Meanwhile, advances in integrated photonics [18-23], driven by the compelling economics of ever smaller footprint and lower power consumption, have created new possibilities and opportunities for RF photonics. Commercialized wafer scale fabrication of III-V, dielectrics, elemental semiconductor and nonlinear crystals have solved key challenges for the co-integration of lasers, modulators, photodetectors, and passive components, and have paved the road for integrated RF photonics to bring it closer towards commercial applications.

As one of the most powerful tools in RF photonic systems, optical frequency combs can serve as multi-wavelength sources and establish multiple RF channels, and thus can greatly increase the capacity for transmission and performance for transversal processers [24-28]. Approaches that use discrete sources for each wavelength have been very successful, such as discrete laser arrays, mode-locked lasers, or cascaded modulators, and yet these methods do have limitations of one form or another, such as the cost, ability to be integrated or the number of available wavelengths, and thus new approaches are needed to overcome these challenges for integrated RF photonic systems.

In 2008-10, new platforms for nonlinear optics, including Hydex [29-38] and silicon nitride [39, 40], were introduced that exhibit negligible nonlinear absorption in the telecom band, a moderate nonlinear parameter and extremely high nonlinear figure of merit, which are ideal for micro-comb generation. Following the first report of Kerr frequency comb sources in 2007 [41], the first integrated CMOS compatible integrated optical parametric oscillators were reported in 2010 [29, 39], and since then this field has exploded [42-50]. Many cutting-edge applications have been demonstrated based on CMOS-compatible micro-combs, ranging from filter-driven mode-locked lasers [47-50] to quantum physics [51-56]. Most recently, Kerr micro-combs have demonstrated their enormous potential for sources for ultrahigh bandwidth coherent optical fiber communications [42, 43]. Meanwhile, for RF photonics, many new applications have been investigated with the fundamental advantages of micro-combs demonstrated [57-60].

In this paper, we demonstrate a reconfigurable RF photonic intensity differentiator [58] based on CMOS-compatible micro-combs. By employing an on-chip nonlinear micro-ring resonator (MRR), we generate a broadband Kerr comb with a large number of comb lines and use it as a high-quality multi-wavelength source for a transversal differentiator. The large frequency spacing of the integrated Kerr comb yields a potential operation bandwidth of over 100 GHz, well beyond dwidth of electronic devices. By programming and shaping the power of individual comb lines

according to corresponding tap weights, reconfigurable intensity differentiators with variable differentiation orders can be achieved. Detailed analyses of the operation principle and experimental demonstrations of fractional-, first-, second-, and third-order intensity differentiations are performed.

2. OPERATION PRINCIPLE

Based on the theory of signals and systems, the spectral transfer function of an *N*-th order temporal differentiator can be expressed as

$$H(\omega) \propto (j\omega)^N, \tag{1}$$

where $j = \sqrt{-1}$, ω is the angular frequency, and N is the differentiation order. According to the above transfer function, the amplitude response of a temporal differentiator is proportional to $|\omega|^N$, while the phase response has a linear profile, with a zero and π jump at zero frequency for N even and odd, respectively. The ideal RF amplitude and phase responses of first-, second-, and third-order microwave differentiators are shown in Figs. 1(a)–(c), respectively.

In this paper, we employ a versatile approach towards the implementation of microwave photonic differentiators based on transversal filters, where a finite set of delayed and weighted replicas of the input RF signal are produced in the optical domain and combined upon detection. The transfer function of a typical transversal filter can be described as

$$H(\omega) = \sum_{n=0}^{M-1} a_n e^{-j\omega nT}, \tag{2}$$

where M is the number of taps, a_n is the tap coefficient of the n^{th} tap, and T is the time delay between adjacent taps. It should be noted that the differentiator designed based on Eq. (2) is an intensity differentiator, i.e., the output RF signal after being combined upon detection yields an exact differentiation of the input RF signal, in contrast to field differentiators that yield the derivative of a complex optical field [61-65]. Figures 1(e)–(f) depict the difference between field differentiation and intensity differentiation.

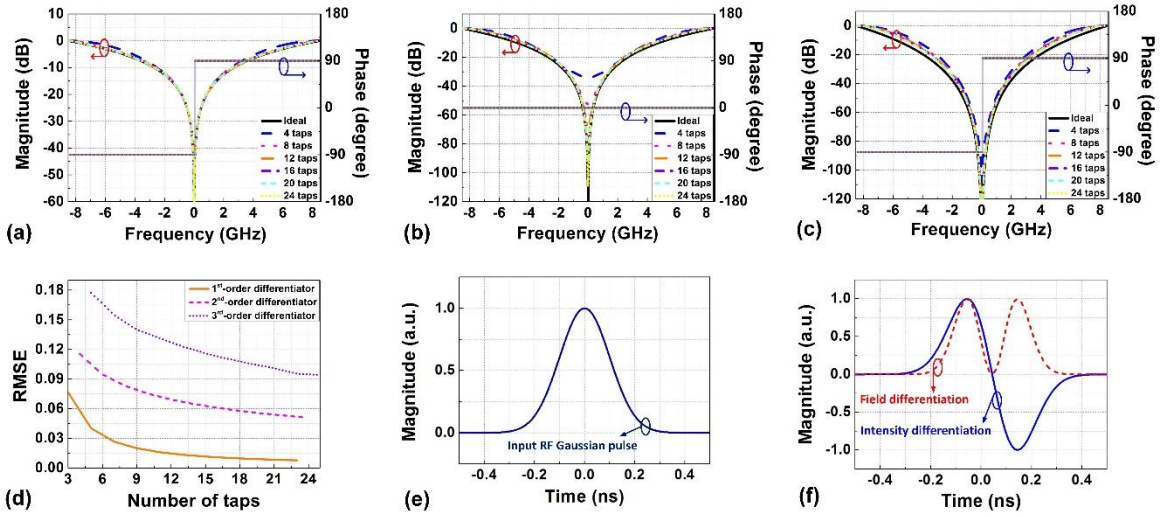

Fig. 1. Simulated RF amplitude and phase responses of the (a) first-, (b) second-, and (c) third-order temporal differentiators. The amplitude and phase responses of the differentiators designed based on Eq. (2) with different number of taps are also shown accordingly. (d) RMSEs between calculated and ideal RF amplitude responses of the first-, second-, and third-order intensity differentiators as a function of the number of taps. Simulated (e) input Gaussian pulse and its corresponding first-order differentiation results.

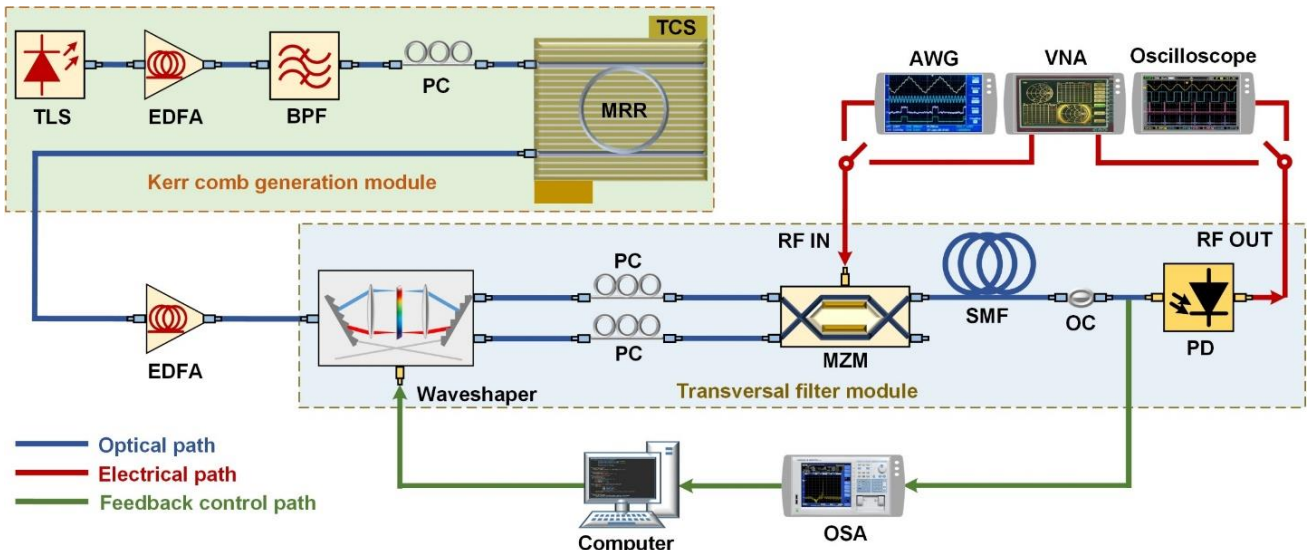

Fig. 2. Schematic illustration of the proposed reconfigurable microwave photonic intensity differentiator. TLS: tunable laser source. EDFA: erbium-doped fibre amplifier. PC: polarization controller. BPF: optical bandpass filter. TCS: temperature control stage. MZM: Mach-Zehnder modulator. SMF: single mode fibre. OC: optical coupler. PD: photo-detector. OSA: optical spectrum analyzer. VNA: vector network analyzer. AWG: arbitrary waveform generator.

To implement the temporal differentiator in Eq. (1), we calculate the tap coefficients in Eq. (2) based on the Remez algorithm [66].The corresponding amplitude and phase responses of the first-, second-, and third-order differentiators as a function of the numbers of taps are also plot in Figs. 1(a)–(c). When the number of taps is increased, it is clear that the discrepancies between the amplitude response of the transversal filters and the ideal differentiators are improved for all three orders, whereas the phase response of the transversal filters is identical to that of the ideal differentiators regardless of the number of taps. To quantitatively analyze the discrepancies in the amplitude response, we further calculate the root mean square errors (RMSEs) for the first-, second-, and third-order differentiators as a function of the number of taps, as shown in Fig. 1(d). One can see that the RMSE is inversely proportional to the number of taps, as reasonably expected. In particular, we note that when the number of taps increases, the RMSE decreases dramatically for a small number of taps, and then decreases more gradually as the number of taps becomes larger.

Figure 2 shows a schematic illustration of the reconfigurable microwave photonic intensity differentiator. It consists of two main blocks: one is a Kerr comb generation module based on a nonlinear MRR and the other is a transversal filter module for reconfigurable intensity differentiation. In the first module, the continuous-wave (CW) light from a tunable laser source is amplified by an erbium-doped fibre amplifier (EDFA), followed by a tunable optical bandpass filter to suppress the amplified spontaneous emission noise. A polarization controller is inserted before the nonlinear MRR to make sure that the polarization state matches the desired coupled mode. When the wavelength of the CW light is tuned to a resonance of the nonlinear MRR and the pump power is high enough for sufficient parametric gain, the optical parametric oscillation (OPO) process in the nonlinear MRR is initiated, which generates a Kerr optical comb with nearly equal line spacing. The nonlinear MRR is mounted on a highly precise temperature control stage to avoid resonance drifts and maintain the wavelength alignment of the resonance to the CW light. Owing to the compact size and ultra-high quality factor of the nonlinear MRR, the generated Kerr comb provides a large number of wavelength channels with narrow linewidths for the subsequent transversal filter module. As compared to conventional intensity differentiators based on laser diode arrays, the cost, size and complexity can be greatly reduced. After being amplified by another EDFA, the generated Kerr comb then is directed to the second module. The Kerr comb is processed by a waveshaper to get weighted taps according to the coefficients calculated by means of the Remez algorithm. Considering that the generated Kerr comb is not flat, a real-time feedback control path is introduced to read and shape the comb lines' power accurately. A 2×2 balanced Mach-Zehnder modulator (MZM) is employed to generate replicas of the input RF signal. When the MZM is quadrature-biased, it can simultaneously modulate the input RF signal on both positive and negative slopes, thus yielding modulated signals with opposite phases and tap coefficients with opposite algebraic signs. After being modulated, the tapped signals from one output of the MZM are delayed by a dispersive fibre. The time delay between adjacent taps is determined jointly by the frequency spacing of the employed comb source and the dispersion accumulated in the fibre.

Finally, the weighted and delayed taps are combined upon detection and converted back into RF signals to form the differentiation output.

It is worth mentioning that due to the intrinsic advantages of transversal filters, this scheme features a high degree of reconfigurability in terms of processing functions and operation bandwidth, thus offering a reconfigurable platform for diverse microwave photonic computing functions. By programming the waveshaper to shape the comb lines according to the corresponding tap coefficients, this scheme can also apply to other computing functions such as Hilbert transforms. The operation bandwidth can also be changed by adjusting the time delay between adjacent taps or employing different tap coefficients. An increased operation bandwidth can be achieved by simply employing a dispersive fibre with shorter length. The operation bandwidth is fundamentally limited by the Nyquist zone, which is determined by the comb spacing. In our case, the frequency spacing of the Kerr comb generated by the nonlinear MRR reaches 200 GHz, thus leading to a potential operation bandwidth of over 100 GHz.

3. EXPERIMENTAL RESULTS

In our experiment, as Fig. 3(a) shows, the nonlinear MRR used to generate the Kerr comb was fabricated on a high-index doped silica glass platform using CMOS compatible fabrication processes. First, high-index (n = 1.7) doped silica glass films were deposited using standard plasma enhanced chemical vapour deposition (PECVD), then photolithography and reactive ion etching (RIE) were employed to form waveguides with exceptionally low surface roughness. Finally, the waveguides were buried in a lower index upper cladding. The radius of the Hydex MRR is ~135 μm. The compact integrated MRR has a large free spectral range (FSR) of ~1.6 nm, i.e., ~200 GHz. Such a large FSR enables an increased Nyquist zone of ~100 GHz, which is challenging for mode-locked lasers and externally-modulated comb sources. The advantages of the platform for integrated nonlinear optics include ultra-low linear loss (~0.06 $dB \cdot cm^{-1}$), a moderate nonlinearity parameter (~233 $W^{-1} \cdot km^{-1}$), and in particular a negligible nonlinear loss up to extremely high intensities (~25 $GW \cdot cm^{-2}$). After packaging the input and output ports of the device with fibre pigtails, the total insertion loss is ~3.5 dB. A scanning electron microscope (SEM) image of the cross-section of the MRR before depositing the SiO_2 upper cladding is shown in Fig. 3(b). By boosting the power of the CW light from the TLS via an EDFA and adjusting the polarization state, multiple mode-spaced combs were first generated, in which the primary spacing was determined by the parametric gain. When the parametric gain lobes became broad enough, secondary comb lines with a spacing equal to the FSR of the MRR were generated via either degenerate or non-degenerate four wave mixing (FWM). In our experiment, the power threshold for the generation of secondary comb lines was ~500 mW.

The resulting Type II Kerr optical comb [67, 68] as shown in Fig. 4(a) is over 200-nm wide, and flat over ~32 nm. Since the generated comb only served as a multi-wavelength source for the subsequent transversal filter in which the optical power from different taps was detected incoherently by the photo-detector, the coherence of the comb was not crucial and the proposed differentiator was able to work under relatively incoherent conditions. In the experiment, the numbers of taps used for fractional-, first-, second-, and third-order differentiation demonstrations were 7, 8, 6, and 6, respectively. The choice of these numbers was made mainly by considering the power dynamic range of the comb lines, i.e., the difference between the maximum power of the generated comb lines and the power associated with the noise floor. The power dynamic range was determined by the EDFA before waveshaping, and in our case, it was ~30 dB. An increased number of taps requires a broader power dynamic range, which can be achieved by using an EDFA with a lower noise floor. As

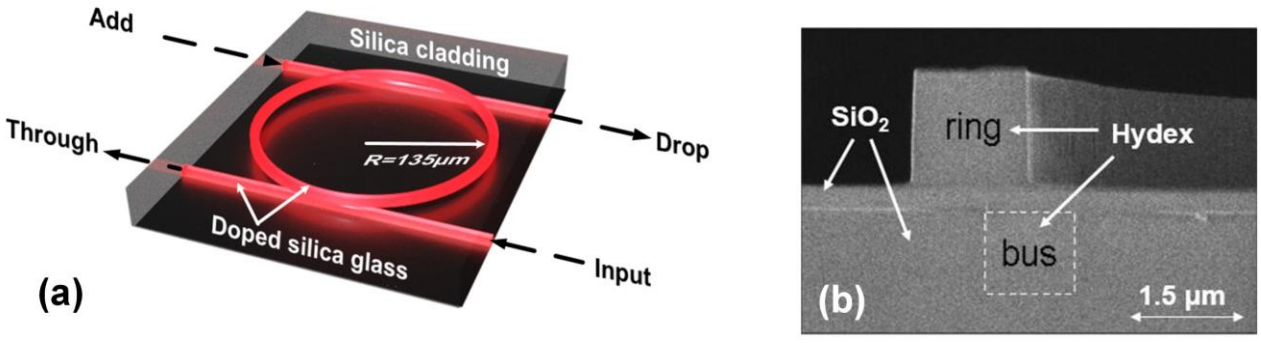

Fig. 3. (a) Schematic illustration of MRR. (b) SEM image of the cross-section of the MRR before depositing the SiO_2 upper cladding.

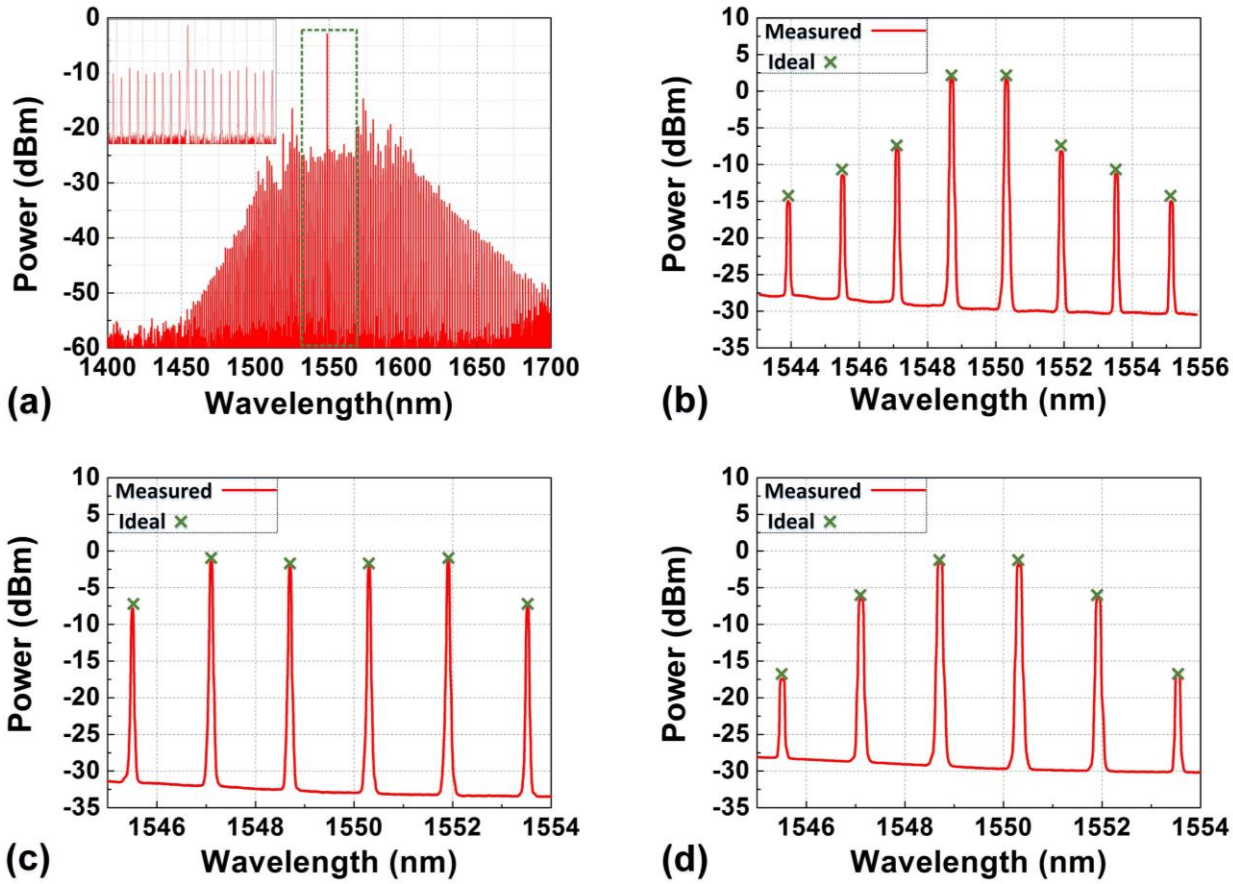

Fig. 4. (a) Optical spectrum of the generated Kerr comb in a 300-nm wavelength range. Inset shows a zoom-in spectrum with a span of ~32 nm. (b)–(d) Measured optical spectra (red solid) of the shaped optical combs and ideal tap weights (green crossing) for the first-, second-, and third-order intensity differentiators.

analysed in section 2, more taps are needed when the differentiation order increases, and for a fixed number of taps, increasing the order of differentiation also increases the required power dynamic range. In order to get better performance with a limited number of taps, we decreased the operation bandwidth of the second- and third-order differentiators to half of the transversal filter's Nyquist frequency when designing the response function with the Remez algorithm. It should be noted that the actual bandwidth of the differentiator is not limited by this design since the FSR of the transversal filter can be enlarged. The calculated tap coefficients for fractional-, first-, second-, and third-order differentiations are listed in Table I. The selected comb lines of the generated optical comb were processed by the waveshaper based on these coefficients. Considering that the generated Kerr comb was not flat, we adopted a real-time feedback control path to increase the accuracy of comb shaping. The comb lines' power was first detected by an optical spectrum analyzer (OSA) and compared with the ideal tap weights, and then an error signal was generated and fed back into the waveshaper to calibrate the system and achieve accurate comb processing. The shaped optical combs are shown in Figs. 4(b)–(d). A good match between the measured comb lines' power (red solid line) and the calculated ideal tap weights (green crossing) was achieved, indicating that the comb lines were successfully shaped. They were then divided into two parts according to the algebraic sign of the tap coefficients and fed into the 2×2 balanced MZM biased at quadrature. The modulated signal after the MZM was propagated through ~2.122-km single mode (dispersive) fibre (SMF). The dispersion of the SMF is ~17.4 ps/(nm·km), which corresponds to a time delay of ~59 ps between adjacent taps and yields an effective FSR of ~16.9 GHz in the RF response spectra.

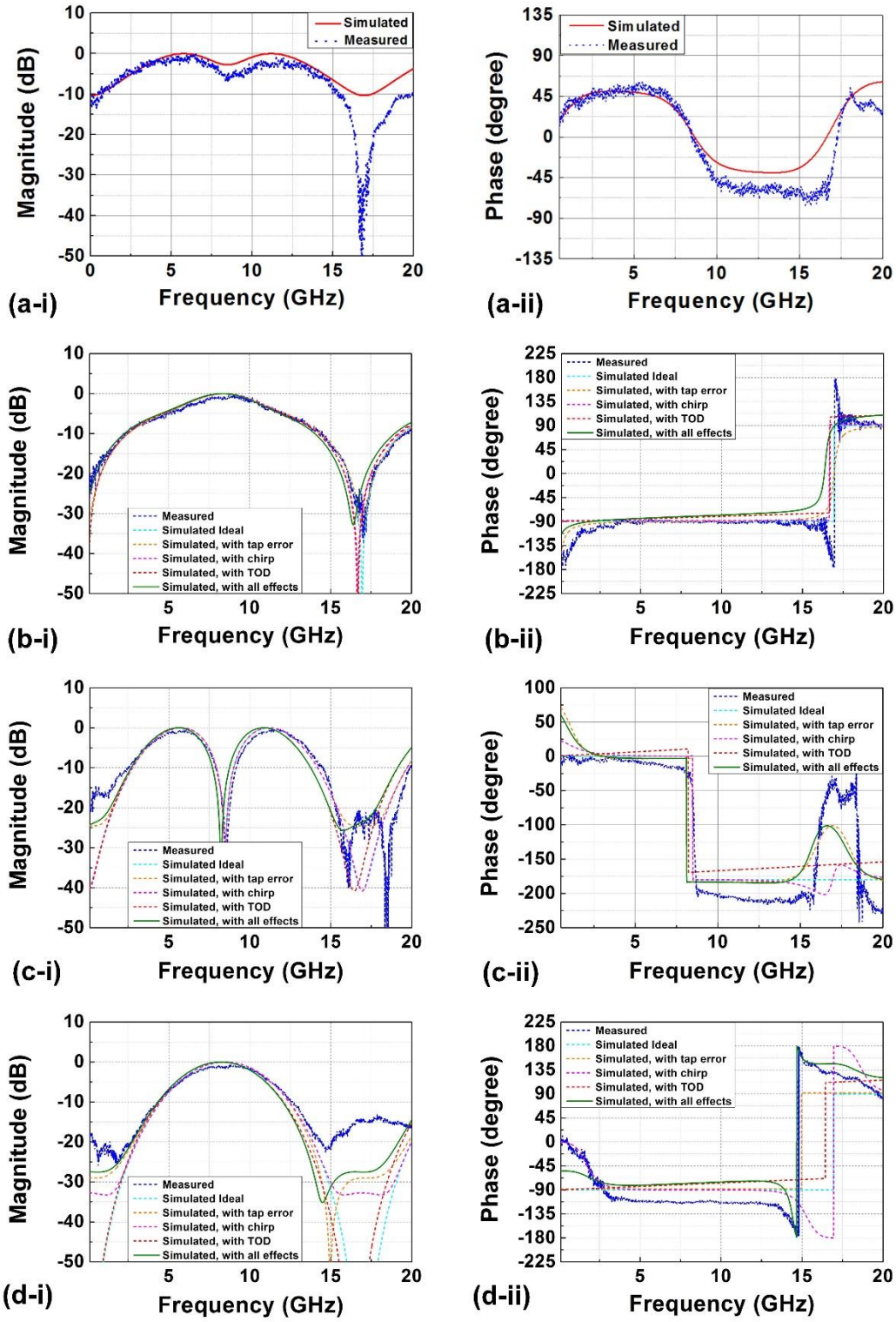

Fig. 5. Measured and simulated RF amplitude and phase responses of (a-i)–(a-ii) the fractional-order, (b-i)–(b-ii) the first-order, (c-i)–(c-ii) second-order, and (d-i)–(d-ii) third-order intensity differentiators. The simulated amplitude and phase responses after incorporating the tap error, chirp, and the third-order dispersion (TOD) are also shown accordingly.

Table 1.

Tap coefficients for the fractional-, first-, second-, and third-order differentiations.

Order of differentiation	Number of taps	Tap coefficients
Fractional-order	7	[0.0578, -0.1567, 0.3834, 1, -0.8288, 0.0985, -0.0892]
First-order	8	[−0.0226, 0.0523, −0.1152, 1, −1, 0.1152, −0.052, 0.0226]
Second-order	6	[0.0241, −0.1107, 0.0881, 0.0881, −0.1107, 0.0241]

After the weighted and delayed taps were combined upon detection, the RF responses for different differentiation orders were characterized by a vector network analyser (VNA, Anritsu 37369A). Figures. 5(a-i), (b-i), (c-i) and (d-i) show the measured and simulated amplitude responses of the first-, second-, and third-order intensity differentiators, respectively. The corresponding phase responses are depicted in Figs. 5(a-ii), (b-ii), (c-ii) and (d-ii). It can be seen that all the three differentiators feature the responses expected from ideal differentiations. The FSR of the RF response spectra is ~16.9 GHz, which is consistent with the time delay between adjacent taps, as calculated before measurement. Note that by adjusting the FSR of the proposed transversal filter through the dispersive fibre or by programming the tap coefficients, a variable operation bandwidth for the intensity differentiator can be achieved, which is advantageous for meeting diverse requirements in operation bandwidth.

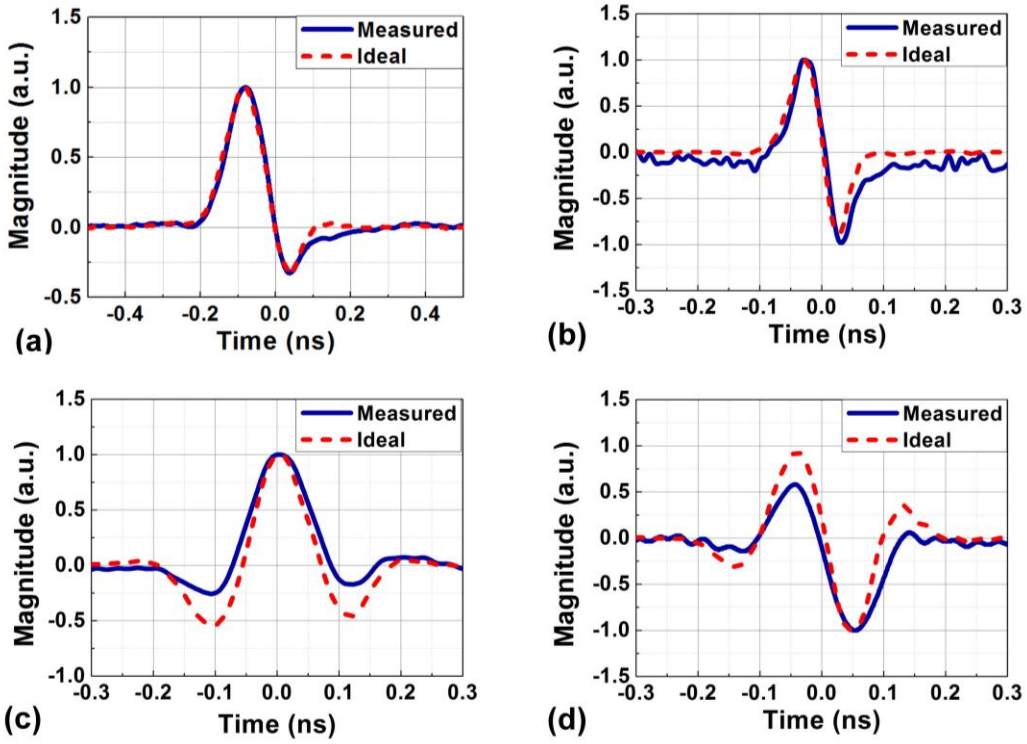

Fig. 6. Theoretical (red dashed) and experimental (blue solid) responses of the (a) fractional- (b) first-, (b) second-, and (c) third-order intensity differentiators.

We also performed system demonstrations of real-time signal differentiations for Gaussian input pulses with a full-width at half maximum (FWHM) of ~0.12 ns, generated by an arbitrary waveform generator (AWG, KEYSIGHT M9505A). The waveform of the output signals after differentiation are shown in Figs. 6(a)–(d) (blue solid curves). They were recorded by means of a high-speed real-time oscilloscope (KEYSIGHT DSOZ504A Infiniium). For comparison, we also depict the ideal differentiation results, as shown in Figs. 6(a)–(d) (red dashed curves). The practical Gaussian pulse was used as the input RF signal for the simulation. One can see that the measured curves closely match their theoretical counterparts, indicating good agreement between experimental results and theory. Unlike the field differentiators, temporal derivatives of intensity profiles can be observed, indicating that intensity differentiation was successfully achieved. For the first-, second-, and third-order differentiators, the calculated RMSE between the measured and the theoretical curves are ~4.15%, ~6.38%, and ~7.24%, respectively.

4. CONCLUSION

We propose and demonstrate a reconfigurable microwave photonic intensity differentiator based on an integrated Kerr comb source. The Kerr optical comb is produced via a CMOS-compatible nonlinear MRR, which greatly increases the processing bandwidth and has the potential for a low cost, size, and complexity processing system. By programming and shaping the individual comb lines' power according to the calculated tap weights, we successfully demonstrate the first-, second-, and third-order intensity differentiations of the RF signal. The RF amplitude and phase responses of the proposed differentiator are characterized, and system demonstrations of real-time differentiations are performed for Gaussian input pulses. We achieve good agreement between theory and experimental results, thus verifying the effectiveness of our method. Our approach provides a new way to implement microwave photonic intensity differentiators featuring with compact device footprint, high processing bandwidth, and high reconfigurability, thus holding great promise for future ultra-high-speed computing and information processing.

5. ACKNOWLEDGMENTS

This work was supported by the Australian Research Council Discovery Projects Program (No. DP150104327). RM acknowledges support by Natural Sciences and Engineering Research Council of Canada (NSERC) through the Strategic, Discovery and Acceleration Grants Schemes, by the MESI PSR-SIIRI Initiative in Quebec, and by the Canada Research Chair Program. He also acknowledges additional support by the Government of the Russian Federation through the ITMO Fellowship and Professorship Program (grant 074-U 01) by the 1000 Talents Sichuan Program. BEL was supported by the Strategic Priority Research Program of the Chinese Academy of Sciences, Grant No. XDB24030000.

References

[1] J. Capmany, and D. Novak, "Microwave photonics combines two worlds," Nature Photonics, **1**(6), 319-330 (2007).

[2] A. J. Seeds, "Microwave photonics," IEEE Transactions on Microwave Theory and Techniques, **50** (3), 877-887 (2002).

[3] R. C. Williamson, and R. D. Esman, "RF photonics," IEEE Journal of Lightwave Technology, **26** (9-12), 1145-1153 (2008).

[4] J. P. Yao, "Microwave Photonics," IEEE Journal of Lightwave Technology, **27** (1-4), 314-335 (2009).

[5] V. R. Supradeepa, C.M. Long, R.Wu, F.Ferdous, E.Hamidi, D.E. Leaird, and A.M. Weiner, "Comb-based radiofrequency photonic filters with rapid tunability and high selectivity," Nature Photonics **6**, 186–194 (2012).

[6] V. Torres-Company and A.M. Weiner, "Optical frequency comb technology for ultra-broadband radio-frequency photonics," Laser & Photonics Reviews **8,** (3) 368-393 (2014).

[7] Q. Z. Cen, Y. T. Dai, F. F. Yin *et al.*, "Rapidly and continuously frequency-scanning opto-electronic oscillator," Optics Express, **25** (2), 635-643 (2017).

[8] J. Dai, X. Y. Xu, J. L. Ke *et al.*, "Self-Oscillating Triangular Pulse Generator Based on 90 degrees Photonic-Assisted Phase Shifter," IEEE Photonics Technology Letters, **29** (3), 271-274 (2017).

[9] J. Dai, X. Y. Xu, Z. L. Wu *et al.*, "Self-oscillating optical frequency comb generator based on an optoelectronic oscillator employing cascaded modulators," Optics Express, **23** (23), 30014-30019 (2015).

[10] K. Xu, R. X. Wang, Y. T. Dai *et al.*, "Microwave photonics: radio-over-fiber links, systems, and applications," Photonics Research, **2** (4), B54-B63 (2014).

[11] X. Y. Xu, J. Dai, Y. T. Dai *et al.*, "Broadband and wide-range feedback tuning scheme for phase-locked loop stabilization of tunable optoelectronic oscillators," Optics Letters, **40** (24), 5858-5861 (2015).

[12] A. X. Zhang, Y. T. Dai, F. F. Yin *et al.*, "Stable radio-frequency delivery by lambda dispersion-induced optical tunable delay," Optics Letters, **38** (14), 2419-2421 (2013).

[13] S. Mansoori, and A. Mitchell, "RF transversal filter using an AOTF," IEEE Photonics Technology Letters, **16** (3), 879-881 (2004).

[14] H. Emami, N. Sarkhosh, L. A. Bui *et al.*, "Wideband RF photonic in-phase and quadrature-phase generation," Optics letters, **33** (2), 98-100 (2008).

[15] S. L. Pan, and J. P. Yao, "Optical generation of polarity- and shape-switchable ultrawideband pulses using a chirped intensity modulator and a first-order asymmetric Mach-Zehnder interferometer," Optics Letters, **34** (9), 1312-1314 (2009).

[16] D. Marpaung, M. Pagani, B. Morrison *et al.*, "Nonlinear Integrated Microwave Photonics," IEEE Journal of Lightwave Technology, **32** (20), 3421-3427 (2014).

[17] D. Marpaung, C. Roeloffzen, R. Heideman *et al.*, "Integrated microwave photonics," Laser & Photonics Reviews, **7** (4), 506-538 (2013).

[18] J. Y. Wu, P. Cao, X. F. Hu *et al.*, "Compact tunable silicon photonic differential-equation solver for general linear time-invariant systems," Optics Express, **22** (21), 26254-26264 (2014).

[19] J. Y. Wu, P. Cao, X. F. Hu *et al.*, "Nested Configuration of Silicon Microring Resonator With Multiple Coupling Regimes," IEEE Photonics Technology Letters, **25** (6), 580-583 (2013).

[20] J. Y. Wu, P. Cao, T. Pan *et al.*, "Compact on-chip 1 x 2 wavelength selective switch based on silicon microring resonator with nested pairs of subrings," Photonics Research, **3** (1), 9-14 (2015).

[21] J. Y. Wu, B. Y. Liu, J. Z. Peng *et al.*, "On-Chip Tunable Second-Order Differential-Equation Solver Based on a Silicon Photonic Mode-Split Microresonator," IEEE Journal of Lightwave Technology, **33** (17), 3542-3549 (2015).

[22] J. Y. Wu, J. Z. Peng, B. Y. Liu *et al.*, "Passive silicon photonic devices for microwave photonic signal processing," Optics Communications, **373**, 44-52 (2016).

[23] J.Wu, T.Moein, X.Xu, G.Ren, A. Mitchell, and D.J. Moss, "Micro-ring resonator quality factor enhancement via an integrated Fabry-Perot cavity", Applied Physics Letters (APL) Photonics, **2** 056103 (2017).

[24] X.Xue and A.M. Weiner, "Microwave photonics connected with microresonator frequency combs", Frontiers of Optoelectronics **9** (2) 238-248 (2016).

[25] O. F. Yilmaz, L. Yaron, S. Khaleghi *et al.*, "True time delays using conversion/dispersion with flat magnitude response for wideband analog RF signals," Optics Express, **20** (8), 8219-8227 (2012).

[26] R. Wu, V. Torres-Company, D. E. Leaird *et al.*, "Supercontinuum-based 10-GHz flat-topped optical frequency comb generation," Optics Express, **21** (5), 6045-6052 (2013).

[27] A. J. Metcalf, V. Torres-Company, D. E. Leaird *et al.*, "High-Power Broadly Tunable Electrooptic Frequency Comb Generator," IEEE Journal of Selected Topics in Quantum Electronics, **19** (6), (2013).

[28] E. Hamidi, D. E. Leaird, and A. M. Weiner, "Tunable Programmable Microwave Photonic Filters Based on an Optical Frequency Comb," IEEE Transactions on Microwave Theory and Techniques, **58** (11), 3269-3278 (2010).

[29] L. Razzari, D. Duchesne, M. Ferrera *et al.*, "CMOS-compatible integrated optical hyper-parametric oscillator," Nature Photonics, **4** (1), 41-45 (2010).

[30] D. J. Moss, R. Morandotti, A. L. Gaeta *et al.*, "New CMOS-compatible platforms based on silicon nitride and Hydex for nonlinear optics," Nature Photonics, **7** (8), 597-607 (2013).

[31] M. Ferrera, L. Razzari, D. Duchesne *et al.*, "Low-power continuous-wave nonlinear optics in doped silica glass integrated waveguide structures," Nature Photonics, **2** (12), 737-740 (2008).

[32] D. Duchesne, M. Ferrera, L. Razzari *et al.*, "Efficient self-phase modulation in low loss, high index doped silica glass integrated waveguides," Optics Express, **17** (3), 1865-1870 (2009).

[33] M. Ferrera, D. Duchesne, L. Razzari *et al.*, "Low power four wave mixing in an integrated, micro-ring resonator with Q=1.2 million," Optics Express, **17** (16), 14098-14103 (2009).

[34] D. Duchesne, M. Peccianti, M. R. E. Lamont *et al.*, "Supercontinuum generation in a high index doped silica glass spiral waveguide," Optics Express, **18** (2), 923-930 (2010).

[35] M. Ferrera, et al., "Ultra-Fast Integrated All-Optical Integrator", Nature Communications, **1** Article 29 (2010). DOI:10.1038/ncomms1028

[36] A. Pasquazi, R. Ahmad, M. Rochette *et al.*, "All-optical wavelength conversion in an integrated ring resonator," Optics Express, **18** (4), 3858-3863 (2010).

[37] A. Pasquazi, Y. Park, J. Azana *et al.*, "Efficient wavelength conversion and net parametric gain via Four Wave Mixing in a high index doped silica waveguide," Optics Express, **18** (8), 7634-7641 (2010).

[38] M. Peccianti, M. Ferrera, L. Razzari *et al.*, "Subpicosecond optical pulse compression via an integrated nonlinear chirper," Optics Express, **18** (8), 7625-7633 (2010).

[39] J. S. Levy, A. Gondarenko, M. A. Foster *et al.*, "CMOS-compatible multiple-wavelength oscillator for on-chip optical interconnects," Nature Photonics, **4** (1), 37-40 (2010).

[40] Ikeda, K., Saperstein, R. E., Alic, N. & Fainman, Y., "Thermal and Kerr nonlinear properties of plasma-deposited silicon nitride/silicon dioxide waveguides", Opt. Express **16**, 12987–12994 (2008).

[41] P. Del'Haye, A. Schliesser, O. Arcizet, T. Wilken, R. Holzwarth, and T. J. Kippenberg, "Optical frequency comb generation from a monolithic microresonator," *Nature* **450**, (7173) 1214-1217 (2007).

[42] P.Marin-Palomo et al., "Microresonator-based solitons for massively parallel coherent optical communications" Nature **546** 274 (2017).

[43] J Pfeifle, V Brasch, M Lauermann, Y Yu, D Wegner, T Herr, K Hartinger, et al., "Coherent terabit communications with microresonator Kerr frequency combs", Nature photonics **8** (5), 375-380 (2014).

[44] P Del'Haye, T Herr, E Gavartin, ML Gorodetsky, R Holzwarth, et al., "Octave spanning tunable frequency comb from a microresonator", Physical Review Letters **107** (6), 063901 (2011).

[45] TJ Kippenberg, R Holzwarth, SA Diddams, "Microresonator-based optical frequency combs", Science **332** (6029), 555-559 (2011).

[46] T Herr, V Brasch, JD Jost, CY Wang, NM Kondratiev, ML Gorodetsky, et al., "Temporal solitons in optical microresonators", Nature Photonics **8** (2), 145-152 (2014).

[47] M.Peccianti, A.Pasquazi, Y.Park, B.E Little, S.Chu, D.J Moss, and R.Morandotti, "Demonstration of an ultrafast nonlinear microcavity modelocked laser", Nature Communications, **3** 765 (2012). DOI:10.1038/ncomms1762

[48] M.Kues, et. al., "Passively modelocked laser with an ultra-narrow spectral width", Nature Photonics, **11** (3) 159 (2017). DOI:10.1038/nphoton.2016.271

[49] A. Pasquazi, L. Caspani, M. Peccianti *et al.*, "Self-locked optical parametric oscillation in a CMOS compatible microring resonator: a route to robust optical frequency comb generation on a chip," Optics Express, **21** (11), 13333-13341 (2013).

[50] A. Pasquazi, M. Peccianti, B. E. Little *et al.*, "Stable, dual mode, high repetition rate mode-locked laser based on a microring resonator," Optics Express, **20** (24), 27355-27362 (2012).

[51] C. Reimer, L. Caspani, M. Clerici *et al.*, "Integrated frequency comb source of heralded single photons," Optics Express, **22** (6), 6535-6546 (2014).

[52] C.Reimer, et al., "Cross-polarized photon-pair generation and bi-chromatically pumped optical parametric oscillation on a chip", Nature Communications, **6** Article 8236 (2015). DOI: 10.1038/ncomms9236

[53] L. Caspani, C. Reimer, M. Kues *et al.*, "Multifrequency sources of quantum correlated photon pairs on-chip: a path toward integrated Quantum Frequency Combs," Nanophotonics, **5** (2), 351-362 (2016).

[54] C. Reimer, M. Kues, P. Roztocki *et al.*, "Generation of multiphoton entangled quantum states by means of integrated frequency combs," Science, **351** (6278), 1176-1180 (2016).

[55] M.Kues, et al., "On-chip generation of high-dimensional entangled quantum states and their coherent control", Nature, **546** (7660) 622-626 (2017).

[56] P. Roztocki, M. Kues, C. Reimer *et al.*, "Practical system for the generation of pulsed quantum frequency combs," Optics Express, **25** (16), 18940-18949 (2017).

[57] T. G. Nguyen, M. Shoeiby, S. T. Chu *et al.*, "Integrated frequency comb source based Hilbert transformer for wideband microwave photonic phase analysis," Optics Express, **23** (17), 22087-22097 (2015).

[58] X.Xu, et al., "Microwave Photonic All-optical Differentiator based on an Integrated Frequency Comb Source", Applied Physics Letters (APL) Photonics, **2** (9) 096104 (2017). DOI: 10.1063/1.4989871.

[59] X. X. Xue, Y. Xuan, H. J. Kim *et al.*, "Programmable Single-Bandpass Photonic RF Filter Based on a Kerr Comb from a Microring," IEEE Journal of Lightwave Technology, **32** (20), 3557-3565 (2014).

[60] Y. C. Han, Z. Li, and J. P. Yao, "A Microwave Bandpass Differentiator Implemented Based on a Nonuniformly-Spaced Photonic Microwave Delay-Line Filter," IEEE Journal of Lightwave Technology, **29** (22), 3470-3475 (2011).

[61] J. Azana, C. Madsen, K. Takiguchi *et al.*, "Guest editorial - Optical signal processing," IEEE Journal of Lightwave Technology, **24** (7), 2484-2486 (2006).

[62] R. Slavik, Y. Park, M. Kulishov *et al.*, "Ultrafast all-optical differentiators," Optics Express, **14** (22), 10699-10707 (2006).

[63] J. Azana, "Ultrafast Analog All-Optical Signal Processors Based on Fiber-Grating Devices," IEEE Photonics Journal, **2** (3), 359-386 (2010).
[64] R. Ashrafi, M. H. Asghari, and J. Azana, "Ultrafast Optical Arbitrary-Order Differentiators Based on Apodized Long-Period Gratings," IEEE Photonics Journal, **3** (3), 353-364 (2011).
[65] R. Ashrafi, and J. Azana, "Figure of merit for photonic differentiators," Optics Express, **20** (3), 2626-2639 (2012).
[66] J. McClellan, T. Parks, and L. Rabiner, "A computer program for designing optimum FIR linear phase digital filters," IEEE Transactions on Audio and Electroacoustics, **21** (6), 506-526 (1973).
[67] T. Herr, K. Hartinger, J. Riemensberger *et al.*, "Universal formation dynamics and noise of Kerr-frequency combs in microresonators," Nature Photonics, **6** (7), 480-487 (2012).
[68] A.Pasquazi, et al., "Micro-Combs: A Novel Generation of Optical Sources", Physics Reports, (2017). DOI:10.1016/j.physrep.2017.08.004.